Applied Surface Science 483 (2019) 10–18

Contents lists available at ScienceDirect

Applied Surface Science

journal homepage: www.elsevier.com/locate/apsusc

Full length article

Opto-chemical control through thermal treatment of plasma enhanced atomic layer deposited ZnO: An *in situ* study

Alberto Perrotta[a,*], Julian Pilz[a], Antonella Milella[b], Anna Maria Coclite[a]

[a] Institute of Solid State Physics, NAWI Graz, Graz University of Technology, Petersgasse 16, 8010 Graz, Austria
[b] Department of Chemistry, Università degli studi di Bari, Via E. Orabona 4, 70126, Bari, Italy

ARTICLE INFO

Keywords:
Zinc oxide
Thin films
Electro-optical materials
Annealing
Plasma
Atomic layer deposition

ABSTRACT

Properties and performance of materials are closely connected. In order to obtain piezoelectric and lasing optical quality, ZnO has to be free of defects and highly crystalline. Instead, conductivity depends upon such defects, making it not trivial to aim at a specific set of properties in a single step. In this regard, we studied *in situ* the effect of temperature as an additional knob to finely control such properties. In this contribution, plasma enhanced atomic layer deposited (PE-ALD) zinc oxide (ZnO) layers, deposited between 25 °C and 250 °C, were studied *in situ* during annealing in air, and the opto-chemical and structural characteristics of the oxides were followed as a function of temperature. *In situ* spectroscopic ellipsometry (SE) and X-ray diffraction (XRD) were adopted to identify temperature windows where major structural and optical changes in the material occurred. Two temperature regions were identified for the effusion of adsorbed gases and minor structural rearrangements (180–280 °C) and for the growth/coalescence of ZnO crystals and its densification (360–500 °C). The results were corroborated by *ex situ* SE, XRD, UV–Vis and X-ray photoelectron spectroscopy. The *in situ* study revealed differences among the ZnO layers deposited at different temperatures, giving additional insights on the material properties deposited by PE-ALD.

1. Introduction

Zinc oxide (ZnO) is a well-studied II-VI semiconductor showing versatile and easy tunable properties, making it the material of choice of an increased number of optoelectronic applications. A number of highly referenced reviews published in the last 10 years well represent the still growing interest in the ZnO properties, processing, and device applications, mostly when deposited as thin film [1–4]. It possesses a wide direct bandgap (~3.37 eV) and large excitonic binding energy (~60 meV) which make it useful for near-UV optoelectronic devices and for lasing applications [5,6]. The high transparency in the visible spectrum and the possibility to tune its electrical properties *via* doping, *e.g.*, aluminum doping [7,8], makes it a valid alternative as a transparent conductive oxide (TCO). The polar nature of ZnO, originating from its wurtzite hexagonal crystal structure, enables piezoelectricity in a high quality material, allowing its use in piezo-sensors and actuators [9].

Atomic layer deposition (ALD), either thermal or enhanced by plasma (PE-ALD), has often been adopted as the method of choice to deliver high quality (ultra-)thin ZnO films [3,10–15]. Polycrystalline thin films were obtained, down to room temperature [16,17]. The optical and structural properties of ZnO have been mainly controlled by adjusting the substrate temperature during the growth, obtaining layers with different preferential crystal orientation and opto-electrical properties [3,14]. A transition from a 100 to a 002 crystal orientation is generally reported as a function of the deposition temperature, both in plasma and thermal ALD [10,14]. Moreover, the optical quality as measured with photoluminescence (PL) has been found to improve with the deposition temperature, due to the removal of defects [16].

Although the materials deposited are of high quality, mostly for low temperature processes, defects and impurities are still introduced in the ZnO structure, posing a limit in their application as piezoelectric or lasing components. Post-deposition annealing is a common method used for enhancing the properties of the ZnO thin films, and recently it has been applied to ALD deposited layers [18–21]. It has been shown that, as a function of the annealing temperature, crystal growth and increased optical density are achieved [19,21], together with an enhanced optical quality of the layer, as witnessed by the more intense photoluminescence [18]. Moreover, next to the classical annealing, increasing interest on the effect of thermal treatments on the properties of the materials have been raised by the possibility of post-deposition high temperature treatments as part of the material synthesis.

* Corresponding author.
E-mail address: a.perrotta@tugraz.at (A. Perrotta).

https://doi.org/10.1016/j.apsusc.2019.03.122
Received 11 January 2019; Received in revised form 4 March 2019; Accepted 13 March 2019
Available online 20 March 2019
0169-4332/ © 2019 The Authors. Published by Elsevier B.V. This is an open access article under the CC BY-NC-ND license (http://creativecommons.org/licenses/BY-NC-ND/4.0/).

Template-assisted growth methods allow the production of complex 3D nanostructures [22–25], usually not achievable by ALD. The removal of an organic template after coating with ALD ZnO is obtained by calcination or annealing, and, in turn, the properties of the remaining material are influenced by the temperature and conditions adopted. In this way, (hollow) nanotubes, nanopillars, and nanofibers of ZnO (among other materials) were achieved, starting from the removal of different templates (*e.g.*, carbon nanotubes, electrospun fibers, bio-nano-templates) [22]. For this application, thorough investigations on the material properties as a function of temperature are paramount for determining *a priori* the opto-chemical and structural properties of the remaining nanostructured material.

Recently, Zheng et al. investigated the effect of different annealing temperature ranges on ALD ZnO thin films by a detailed spectroscopic ellipsometry study [19]. Three different regions were identified where the optical and structural properties of ZnO were found to drastically change, namely below 400 °C, 400–700 °C, and 700–900 °C. The second region was deemed responsible for the major structural changes in ZnO thin films, while in the third region degradation of the materials occurred. Similar conclusions were drawn in other studies on ALD ZnO layers, adopting among others atomic force microscopy [21], X-ray diffraction and reflectivity [18,20], and photoluminescence [18,21]. In all of the studies presented, the layers were measured *ex situ*, that is, after annealing and at room temperature. Furthermore, generally only a single ALD ZnO deposition parameter (*e.g.*, temperature) was investigated.

In this contribution, plasma enhanced ALD was adopted for the deposition of ZnO at temperatures ranging between 25 and 250 °C. The annealing procedure in air was followed *in situ* by means of spectroscopic ellipsometry (SE) and X-ray diffraction (XRD). The evolution of the optical and structural properties was then followed during the annealing and temperature windows responsible for the enhancement of the material properties were identified. The study is corroborated by *ex situ* techniques, highlighting the possibility of obtaining specific material properties as a function of the annealing temperature. The investigation of the annealing effect on different ZnO layers highlighted differences in the material characteristics not detectable from the pristine layers.

2. Experimental section

A custom-built direct plasma ALD reactor was used to deposit the ZnO thin films on single side polished *c*-Si (100) substrates (Siegert Wafer). The reactor was in an asymmetrical plate configuration, in which the showerhead radio frequency (RF) electrode and ground electrode had a distance of 8 cm and are 20 cm and 30 cm in diameter, respectively. Diethyl zinc (DEZ, Sigma-Aldrich, CAS 557-20-0) was used as the metalorganic precursor. The input power was supplied by an RF-power generator (Advanced Energy Cesar 13.56 MHz) through a matching network (Advanced Energy Navio). An input power of 60 W was chosen for these experiments [17]. The pressure in the reactor was controlled *via* an automatized butterfly valve (MKS 253B). The valve was set to a fixed opening in order to reach a pressure of around 85 mTorr during plasma exposure. A multi gas controller (MKS 647C) and mass flow controllers (MKS MF1-C) were used to control the flow rates of the gases. Pure oxygen was used during the plasma step and Ar was adopted in the purging step. The flow rates for O_2 and Ar were set at 20 sccm during the plasma and the purging step, respectively. An ALD-valve (Swagelok ALD3) was used to pulse DEZ into the reactor. Due to the high vapor pressure of DEZ, no further heating or bubbling system were adopted. The depositions were carried out in a range of temperature going from 25 to 250 °C [17].

Spectroscopic ellipsometry (J.A. Woollam M-2000 V) was used to determine the thickness and optical properties of the films after deposition. The measurements were carried out at three different angles (65°, 70°, and 75°) in a wavelength range from 370 to 1000 nm. The analysis of the spectra was performed with the software CompleteEASE®. The thickness was determined by applying a three-layer model consisting of a semi-infinite silicon substrate, a native silicon oxide layer with a fixed thickness of 1.5–2 nm, and a Cauchy layer, as follows

$$n(\lambda) = A + \frac{B}{\lambda^2} + \frac{C}{\lambda^4} \quad (1)$$

in which n is the wavelength-dependent refractive index, λ is the wavelength and A, B, and C are fit parameters. An Urbach tail was used to account for absorption at lower wavelength. The fitting was limited to the transparent region of ZnO, *i.e.*, 450–1000 nm.

In order to determine the bandgap and absorption coefficient of ZnO layers, an oscillator model was also adopted, extending the wavelength range to 370–1000 nm. The oscillator model consisted of Gaussian oscillators to account for the high- and near infrared-energy contributions and a PSEMI-M0 model to account for the near-bandgap absorption. The PSEMI-M0 model is an oscillator with a sharp onset and Kramers–Kronig consistent properties consisting of four connected polynomial spline functions. It is modeled by fit parameters controlling the amplitude, broadening, center energy, left and right endpoints, and left and right midwidth control points [26]. The bandgap energy was obtained by extrapolating the linear part from a Tauc-plot [27].

For the *in situ* temperature-dependent studies, the SE system was equipped with a THMS600 temperature stage (Linkam, UK), equipped with a sealing capping chamber. Dry air was continuously flown into the capping chamber, kept at atmospheric pressure. The temperature was varied from room temperature to 600 °C at 30 °C/min. The temperature was then kept constant at 600 °C for 100 min. Subsequently, the system was let cool down to temperatures of 30–40 °C, with the same rate. For these experiments, the acquisition angle was fixed at 70°.

X-ray diffraction (XRD) in a θ/θ-configuration was performed to analyze the crystalline properties of the films in the specular direction. The diffractometer (Panalytical Empyrean) used the radiation of a copper tube monochromatized with a layered X-ray mirror (λ = 1.5418 Å) and a PIXcel^{3D}-detector which was operated in 1D-mode. A 1/8° divergence, a 10 mm mask, and a P7.5 anti-scatter slit were used in the setup. *In situ* temperature-dependent XRD studies were performed with a DHS900 heating stage attachment (AntonPaar, Austria), using a heating rate of 30 °C/min. The integration time was set to 3 min/measurement [28]. All data were recorded using the same setup and are represented in the scattering vector (q_z) notation, where $q_z = 4\pi \cdot \sin(\theta)/\lambda$.

Surface chemical composition was investigated by X-ray Photoelectron Spectroscopy (XPS). Analyses were performed with a Scanning XPS Microprobe (PHI 5000 Versa Probe II, Physical Electronics), equipped with a monochromatic Al Kα X-ray source (1486.6 eV) operated at 15 kV with a spot of 100 μm and a power of 24.8 W. Survey (0–1200 eV) and high resolution spectra were recorded in FAT (Fixed Analyzer Transmission) mode at a pass energy of 117.40 and 29.35 eV, respectively. In the set conditions, the analyzer energy resolution (FWHM, full width at half-maximum height), measured on the silver Ag 3d5/2 photoemission line, was 0.7 eV for a pass energy of 29.35 eV. All spectra were acquired at a take-off angle of 45° with respect to the sample surface. Surface charging was compensated using a dual beam charge neutralization, with a flux of low energy electrons (~1 eV) combined with very low energy positive Ar ions (10 eV). Samples were sputter cleaned for 1 min with an Ar ion beam of 1 KV, 1 μA (raster size: 2 × 2 cm^2). The acquired spectra were processed with CasaXPS software. The lattice O—Zn component of the O1s spectrum was used as internal standard for charging correction and it was set to 529.8 eV [29].

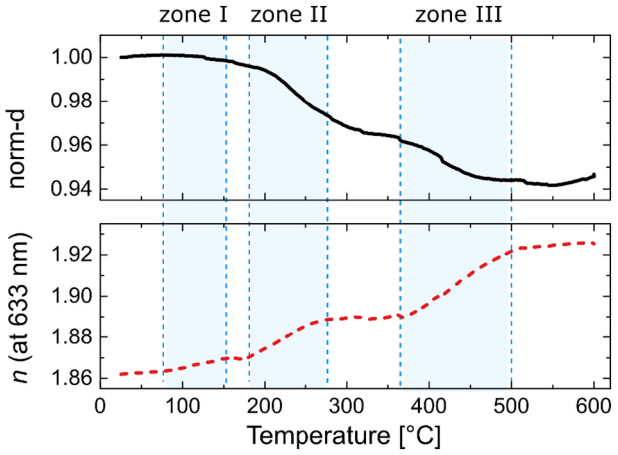

Fig. 1. Normalized thickness (norm-d) and refractive index (*n*, at 633 nm) of PE-ALD ZnO deposited at 25 °C reported as a function of the annealing temperature during *in situ* SE measurements. The three main regions affected by the annealing procedure are also highlighted. The error on norm-d is ± 0.01 (± 0.3 nm); the error on the refractive index is ± 0.001.

3. Results and discussion

3.1. Room temperature ZnO: in situ investigation

ZnO layers of 30 nm in thickness were deposited with PE-ALD at room temperature, following the procedure already reported [17]. In order to measure the evolution of the optical properties of the materials as a function of the annealing temperature, the layers were investigated *in situ* with spectroscopic ellipsometry and X-ray diffraction. In Fig. 1, the normalized thickness (norm-d) and the refractive index (*n*, at 633 nm) measured *in situ* are reported as a function of the annealing temperature.

The refractive index before annealing was 1.862 ± 0.005. The value is in line with previously reported PE-ALD ZnO [17]. Three main zones were identified as a function of temperature, and highlighted in Fig. 1. In zone I (75–160 °C), removal of adventitious carbon and impurities present on the surface of the sample is suggested. The refractive index was found to slightly increase, due to the removal of less optically dense material from the surface of the ZnO layer. Consequently, the thickness is reduced of < 1%, in line with the removal of surface contaminations. Significant changes in the material optical constants and thickness started in zone II (170–280 °C). In this temperature range, a total reduction of 3.5% of the film thickness was witnessed, together with an increase in refractive index, up to values of 1.889 ± 0.005. The change in optical properties in this temperature range is attributed to the partial removal of carbon contaminations: Carbon contaminations with an atomic percent of 2.6% were measured by XPS. Moreover, additional ZnO is consequentially formed in the presence of an oxidative environment. In the literature, effusion experiments carried out on ALD ZnO deposited also at room temperature pointed out the effusion of water and hydrogen from the layers in the same temperature range, above 150 °C [30]. Particularly, layers deposited at room temperature showed the highest amount of incorporation within the ZnO matrix of volatile gases, which would support the significant changes measured by *in situ* SE here reported for Zone II.

A further increase in temperature identifies a third region (Zone III, Fig. 1), between 375 °C and 500 °C. The refractive index is found to increase up to values of 1.926 ± 0.005, and the thickness to decrease of 6%. In the literature, Zheng et al. [19] reported on the effect of annealing on thermal ALD ZnO as measured with spectroscopic ellipsometry. Comparable results in terms of thickness loss are obtained for ZnO deposited at 150 °C in the same annealing temperature range. The authors attributed the decrease in thickness to preferential evaporation of ZnO. In the present case, evaporation of ZnO is excluded due to the generally higher temperature at which this evaporation is known to occur (> 600 °C) [31,32]. Furthermore, the thickness was found not to significantly change between 500 °C and 600 °C, inferring the total removal of contaminants from the layers in this temperature range. The increase in refractive index can be attributed to the final removal of the less dense carbon-containing groups and formation of denser ZnO. Furthermore, recrystallization and growth of ZnO crystals are also reported to occur in this temperature range, contributing to the increase in refractive index of the layers [19]. In between Zone II and Zone III, the refractive index stayed constant and the thickness was found to decrease of < 1% up to 300 °C. The mismatch in the two properties is an indication of different mechanisms affecting the layers, additionally highlighting the robustness of the model used, with no correlation among the optical parameters chosen. The refractive index increase is more likely related to structural variations, such as condensation of adjacent Zn-OH groups, with formation of water [33], or relaxation of residual stress due to effusion of gases from grain boundaries regions. Thickness variation, in addition of being strongly correlated with the aforementioned effects, is also affected by surface removal of the effusive gases, in turn accounting for the residual thickness variation.

Next to thickness and refractive index, the extinction coefficient was also followed as a function of the annealing temperature as reported in Fig. 2a.

As shown in Fig. 2a, *k* values are found to significantly increase in the region close to the ZnO bandgap (3.3 eV, 375 nm). In order to

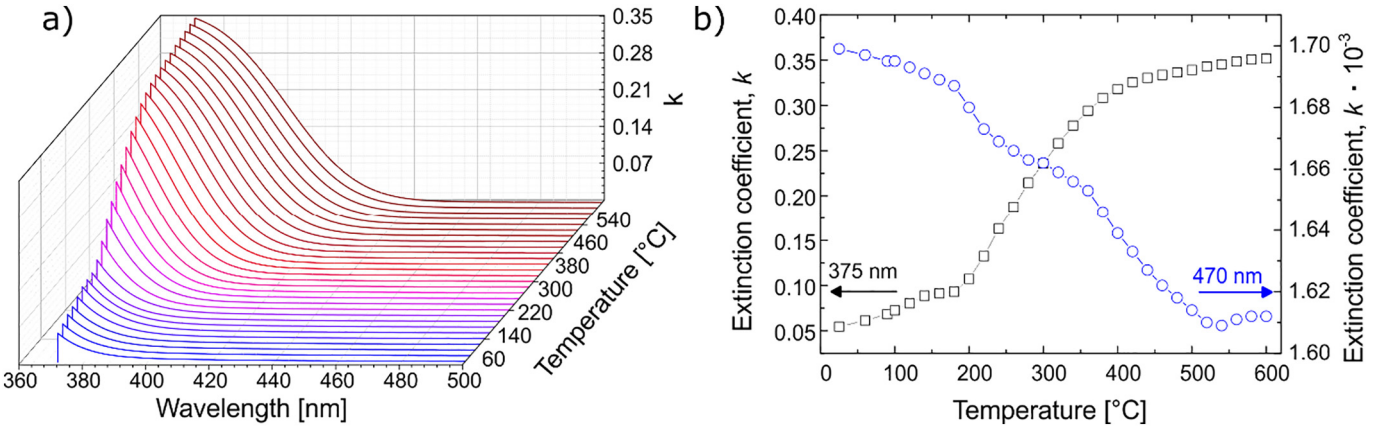

Fig. 2. a) Extinction coefficient (*k*) measured *in situ* as a function of the annealing temperature in the wavelength range 370–500 nm and b) single wavelength *k*-values as a function of temperature at 375 nm (black squares), theoretical bandgap of the bulk single crystal ZnO, and at 470 nm (blue circles). The error on the extinction coefficient is in the order of ± $3 \cdot 10^{-5}$.

understand the effect of temperature on the k values, these need to be correlated with the absorption of the material. The extinction coefficient is related to the absorption coefficient (α) by:

$$\alpha(\lambda) = \frac{k(\lambda) \bullet 4\pi}{\lambda} \tag{2}$$

so being directly correlated with the absorption of the material at a specific wavelength. The increase in k at the bandgap value is therefore attributed to the absorption edge moving to the lower energy region with increasing temperature, as shown in Fig. 2b. For polar semiconductors, such as ZnO, the increase in k is attributed to a combination of the thermal effect and the Urbach effect, that is, the temperature dependent exponential increase of the absorption edge (Urbach tail) below the energy band gap, leading to a broadening of the region of absorption caused by the lattice vibrations [34,35]. Hence, structural changes during annealing are occurring in conjunction with the classical temperature effects on semiconductors and are therefore difficult to differentiate. In order to exclude thermal effects, the value of k was also followed at higher wavelength, namely 470 nm (see Fig. 2b). At this wavelength, absorption can be mainly attributed to impurities and structural defects [19], thus better highlighting the effect of temperature on the quality of the ZnO thin films. As shown in Fig. 2b, k values (at 470 nm) are found to decrease as a function of the annealing temperature, confirming the origin of the variations to be solely attributed to irreversible structural changes. As already mentioned for the refractive index and thickness, three main regions can be identified also in the k-trends. As previously seen in Fig. 1, Zone I only slightly affects the optical properties. Zone II and zone III (already identified in Fig. 1), in the temperature range 170–280 °C and 375–500 °C, respectively, show a steep decrease in the extinction coefficient. Removal of carbon species and defects, deemed responsible for absorption below the bandgap, can be accounted for such a decrease, pointing out an increased optical quality of the material as a function of the annealing temperature. Moreover, presence of amorphous regions could also account for absorption below the bandgap, and recrystallization of ZnO, known to occur in the range 360–450 °C, would lead to a decrease of the absorption below the bandgap, confirming the conclusions drawn from the variation of thickness and refractive index.

In order to follow the evolution of the optical bandgap with temperature, a Tauc plot was derived from the absorption coefficient, calculated from k adopting Eq. (2) (see The Supporting Information, Fig. S2) and the bandgap values were extrapolated from the linear part of the curve. The bandgap, measured *in situ* during the annealing, is presented in Fig. 3.

The temperature variation of the bandgap can be modeled by the Varshni equation for semiconductors, that is:

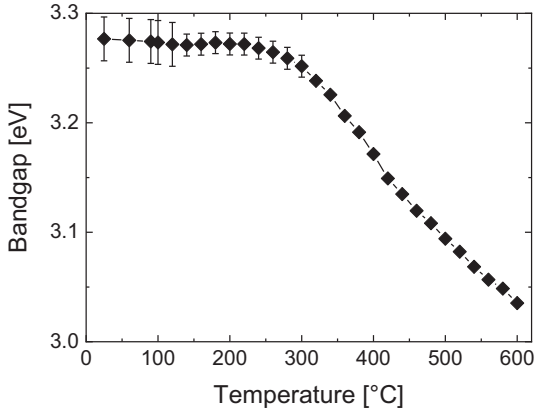

Fig. 3. Bandgap of the ZnO layers as a function of temperature as extrapolated from the Tauc plots obtained from the absorption coefficient.

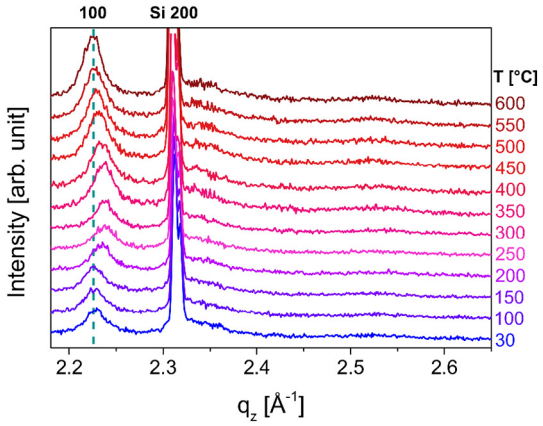

Fig. 4. *In situ* XRD measurements performed during the annealing procedure of the PE-ALD ZnO between 30 °C and 600 °C. Bragg peaks originating from ZnO and Si are indicated by their respective HKL values.

$$E_g(T) = E_g(0) - \frac{\alpha T^2}{T + \beta} \tag{3}$$

where $E_g(0)$ is the bandgap at T = 0, α and β are constants [36–38]. In order to better highlight the major structural variations occurring during annealing, the plot in Fig. 3b was modeled with Eq. (3). The fitting (see The Supporting Information Fig. S3) shows the incompatibility of the classical models for semiconductors for the PE-ALD ZnO during the annealing procedure. The Varshni model is only able to fit the bandgap values up to 150 °C, at the beginning of the first temperature window which showed optical changes with SE (see Fig. 1).

Next to the *in situ* investigation of the optical properties, the PE-ALD ZnO was followed with *in situ* XRD measurements, showed in Fig. 4.

In a reference ZnO powder (26170-ICSD [39]), peaks are generally observed at q_z positions of 2.23 $Å^{-1}$, 2.41 $Å^{-1}$, and 2.54 $Å^{-1}$, which match with the (100), (002), and (101) diffraction, respectively. The position of the Bragg peak corresponding to the (100) orientation is indicated in Fig. 4 as a guide to the eye. The pristine PE-ALD ZnO deposited at room temperature (represented in the plot in Fig. 4 as the diffractogram measured at 30 °C) shows a preferential orientation along the [100] direction, as previously reported [17]. The crystallite orientation is kept throughout the annealing procedure and no additional peaks appeared. In agreement with the optical properties as a function of temperature, the Bragg peak was found to change in specific temperature intervals. Up to 150 °C, no change in position or shape of the 100 peak was witnessed, in line with the band gap values with annealing temperature (Fig. 3). Starting from 200 °C, a shift of the 100 peak to higher q_z was measured, corresponding to a decrease of the lattice spacing [40]. Removal of material and the corresponding decrease in thickness and ZnO densification (as witnessed by SE) creates a compressive stress in the layer along the c-axis, in turn reducing the lattice spacing in the ZnO. As aforementioned, effusive experiment on ALD ZnO deposited at different temperatures showed that, for layers deposited at room temperature, effusion of water was measured starting above 150 °C, which could also account for the development of compressive stress [30]. The intensity and width of the peaks do not change in this temperature region, indicating that the crystallite size and overall crystallinity of the ZnO are not affected. Starting at 350 °C, a rapid increase of the intensity of the 100 peak was measured, indicating an increase in the crystallinity of the ZnO layer. This temperature range is in agreement with the beginning of the increase in refractive index measured in Zone 3 (see Fig. 1). The Bragg peak is found to steadily shift to low q_z, that is, an increase of the lattice spacing. The steady increase was attributed to the thermal expansion of the ZnO, more prominent at higher temperatures. The crystallite size, as measured adopting the Scherrer equation, shows an increase in the crystallite size

ranging from 26.2 nm at room temperature to 31.5 nm at 600 °C. The increase in overall crystallinity and crystallite size can be attributed to the crystallization of amorphous regions (apparent in non-annealed samples) and coalescence of small crystallites [18,19,41]. The combination of SE and XRD better clarifies the nature of the changes in the ZnO layer. The variation in the optical properties (refractive index and optical bandgap) with annealing temperatures up to 350 °C are mainly attributed to removal of impurities from the ZnO layer, together with the development of compressive stress. Starting from 350 °C, recrystallization of amorphous regions of the ZnO and coalescence of smaller crystallites occurs, causing a further densification of the layer, as witnessed by the increase in refractive index (see Fig. 1). The absorption for energies below the bandgap is found to decrease more prominently when the recrystallization of the ZnO occurs. In the same fashion, higher absorption at the bandgap, indicating an increase in the quality of the ZnO, is witnessed in the same temperature range (See Figs. 2 and 3).

3.2. Room temperature ZnO: ex situ investigation

In order to further corroborate the results obtained with *in situ* SE and XRD, *ex situ* characterization of the layers was performed, adopting SE, XRD, and UV–Vis spectroscopy. In Fig. 5, the SE and UV–Vis measurements are reported.

Fig. 5a shows the evolution of the extinction coefficient k after annealing at 100, 200, 400, and 600 °C. Up to 200 °C, no major variation of the k value was measured. Above 200 °C, the extinction coefficient is found to increase around the theoretical value of the ZnO bandgap of 375 nm, indicating a sharper transition and, in turn, enhanced optical properties of the material. These results are in agreement with the *in situ* investigation, showing that the structural changes in the ZnO layers are irreversible and can be tailored as a function of the annealing temperature to meet specific material requirements. In Fig. 5b, the UV–Vis absorption spectra are reported. The spectra show the optical bandgap of ZnO at different annealing temperatures. Increasing the temperature, the bandgap is found to lose near edge absorption, resulting in sharper transitions. The absorption edge was found to shift toward lower energy (red-shift) with the annealing temperature. Red-shift has been reported in the literature for solution and vapor-processed ZnO upon annealing, and it was attributed to the removal of defects and the increase of the crystallite size of the ZnO [42–44]. This is in agreement with the *in situ* SE and XRD results, pointing out material densification and increase in crystallite size. Moreover, with a large free exciton binding energy, ZnO films with good structural quality can show a free excitonic absorption also at room temperature [34,35,45]. The layers deposited at room temperature and before annealing do not show the excitonic absorption. The band edge is smooth, highlighting a high number of defects resulting in near band edge absorption. The appearance of the exciton peak close to the bandgap typical of ZnO was witnessed after annealing above 400 °C, pointing out a correlation between the recrystallization and the optical quality of the material.

By adopting a Tauc plot (see The Supporting Information, Fig. S4) the optical bandgap of the thin films was extrapolated from the linear regions for both SE and UV–Vis measurements (Fig. 5c). The mismatch between the two optical methods arises from the limited region of the bandgap measured with SE, which introduces a systematic overestimation up to 40 meV in the bandgap values. Nevertheless, the two techniques highlight similar aspects of the effect of the annealing on the ZnO optical properties. Up to 200 °C the bandgap was found to increase of about 30 meV (with UV–Vis). Increase in the bandgap was attributed to the removal of loosely bound carbon impurities (see elemental analysis, Table 1) as well as possible elimination of water and interstitial adsorbed oxygen, all introducing near band edge adsorption. At 400 °C, recrystallization of ZnO brings to a red-shift of the bandgap value while a further increase in temperature does not bring major structural changes in the ZnO thin films, as also witnessed by *in situ* SE and XRD.

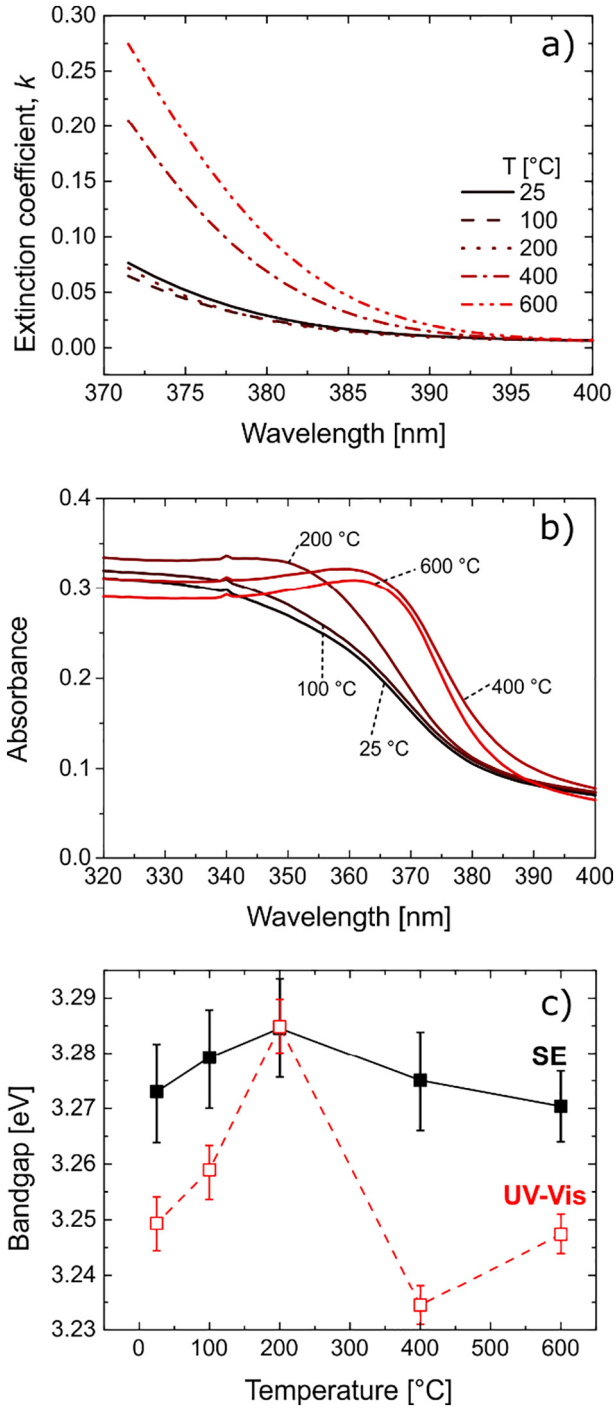

Fig. 5. a) Extinction coefficient (k) as a function of the annealing temperature in the wavelength range 370–500 nm. The measurements were carried out at room temperature after an annealing step at the temperature indicated in the plot. b) Absorbance of the PE-ALD ZnO layers deposited at 25 °C after annealing at different temperatures as measured by UV–Vis spectroscopy; it is worth noticing the presence of an artifact at 340 nm for all the spectra. c) bandgap of the PE-ALD ZnO after annealing at different temperatures as derived from SE and UV–Vis measurements.

3.3. Annealing of high-temperature-deposited ZnO

The effect of annealing in air was also measured on ~30 nm thick

Table 1
Chemical composition of the PE-ALD layers as measured by XPS as a function of the deposition temperature.

Deposition temperature [°C]	Zn [at.%] ± 0.5%	O [at.%] ± 0.5%	[O]/[Zn]	C [at.%] ± 0.5%
25	47.6	51.6	1.084	2.6
50	48.8	51.1	1.048	< 1%
100	47.9	51.1	1.067	< 1%
150	48.1	50.9	1.057	< 1%
200	47.7	51.6	1.081	< 1%
250	47.7	51.5	1.081	2

PE-ALD ZnO deposited at higher temperatures, between 50 °C and 250 °C, and differences in material composition and quality were highlighted. The elemental composition of the layers is reported in Table 1. In Fig. 6, the *in situ* (normalized) thickness (Fig. 6a) and the post-annealing *ex situ* absorption coefficient measured by SE at the ZnO theoretical bandgap (375 nm, Fig. 6b) are reported.

The *in situ* thickness variation as a function of the annealing temperature highlights differences in the quality of the ZnO layers. ZnO deposited at 50 °C has a thickness profile that resembles the one for room-temperature deposited ZnO (see Fig. 1). In the temperature ranges identified in the previous section as Zone 2 and Zone 3, the thickness was found to drop, pointing out removal of impurities and densification/recrystallization of the layers, respectively. This is also confirmed by the increase in absorption at the bandgap after annealing (Fig. 6b) and the increase in refractive index (see The Supporting Information Fig. S5). Thickness loss of 6% was found for the 50 °C-PE-ALD-ZnO after annealing at 600 °C, comparable to the thickness loss of the room-temperature-deposited ZnO. As the deposition temperature increased, the effects of the annealing were less pronounced. As shown in Fig. 6a, the thickness loss in the temperature range 200–300 °C was found to gradually disappear, pointing out the absence of loosely bound impurities in the layer when deposited at higher temperatures. Thickness loss was found to decrease, from 6% (at 50 °C deposition temperature) to < 2% (at 200 °C deposition temperature), and thermal expansion was also witnessed for layers deposited at 150 and 200 °C, inferring a higher ZnO quality in this deposition temperature range. Layers deposited at 250 °C showed a higher thickness loss (3%), due to the presence of carbon contaminations (see Table 1). Differences in the layers are also highlighted in Fig. 6b. The absorption coefficient was found to increase for all the deposition temperatures investigated, and the difference after annealing was found to decrease, pointing out better ZnO quality up to 200 °C, while decreasing again at 250 °C, confirming the conclusions drawn from the *in situ* SE measurements. It is worth mentioning that a variation of roughness, as measured by X-ray reflectivity before and after annealing (Table 1s, Supporting Information) does not contribute to the thickness drop as measured by SE. The roughness values were measured up to 2.2 nm before annealing, slightly increasing to 2.5 nm after annealing. Bandgap values were also calculated from the SE measurements (see The Supporting Information Fig. S6 and S7), showing in this case a blue-shift in the bandgap value. The blue shift was attributed to the presence (and, in turn, removal upon annealing) of a lower amount of impurities and near-band-edge adsorption states, due to the better ZnO quality when deposited at higher temperatures. Moreover, the higher quality of the layers deposited at higher temperature was also confirmed by the applicability of the Varshni equation as a function of temperature. An example is presented in Fig. S8. Increased quality with annealing was also witnessed with XPS measurements, which showed a general increase of the O/Zn ratio (see The Supporting Information Fig. S9) due to the annealing in oxidative ambient, providing more oxygen to the layers, in turn contributing to the recrystallization of ZnO. The atomic composition and the relative content are presented in Table 1.

The crystal structure of the pristine and annealed ZnO was also investigated. The diffractograms of the ZnO layers before and after annealing are presented in Fig. 7.

In Fig. 7, also the diffractograms of the ZnO layer deposited at room temperature are reported as comparison. As a function of temperature, in the pristine layers a transition from a [100] to a [002] preferential direction of the crystallite growth was observed, in line with previous literature on ZnO [10,16]. For all the samples investigated, the peak attributed to the preferential growth direction is shifted at lower q values, that is, the distance between the crystalline planes is larger. After annealing, a shift of the major peak toward higher value of q suggests the release of residual compressive stress in the films with temperature. Moreover, increase in the intensity of the peak suggests the presence of amorphous regions in the pristine films, which are recrystallized after annealing. Coalescence of smaller grains and crystallite growth due to the presence of the amorphous regions is also pointed out by the decrease in peak width, as also aforementioned for the *in situ* XRD on the room temperature ZnO layer. The lattice constants and the residual stress before and after annealing were calculated from the XRD diffractograms. The lattice constants a and c of the wurtzite ZnO structure were calculated using the Bragg's law for first order diffraction. In this case, the plane distance, d, can be written in terms of Miller indices (h, k, and l) and lattice constants (a and c): [41,43].

$$\frac{1}{d_{hkl}^2} = \frac{4}{3}\left(\frac{h^2 + hk + k^2}{a^2}\right) + \frac{l^2}{c^2} \quad (4)$$

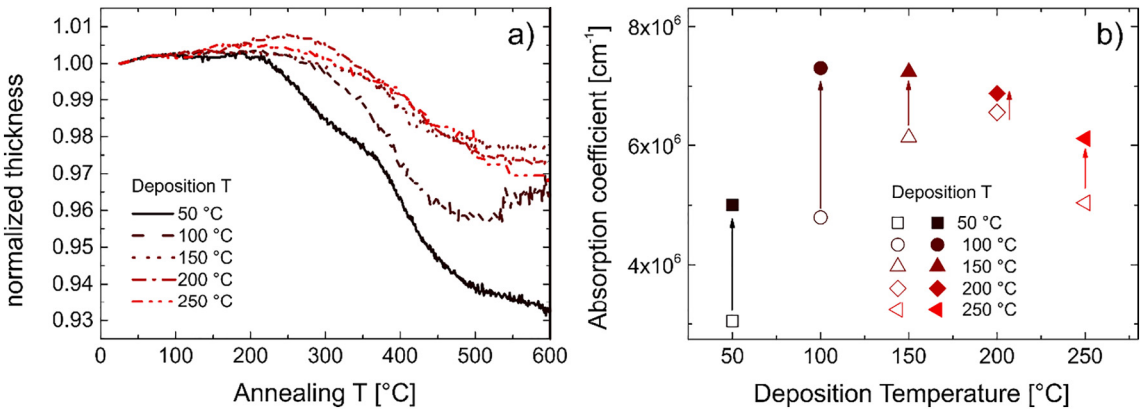

Fig. 6. a) *In situ* normalized thickness followed by SE during the annealing procedure in air for PE-ALD ZnO layers deposited between 50 °C and 250 °C. All layers had a thickness of 30 ± 3 nm and the values are reported as normalized for the sake of clarity. The error on every single curve is in the order of ± 0.3 nm (± 0.01 in normalized thickness). b) absorption coefficient calculated form the k values as measured by SE at 375 nm. Empty and filled symbols refer to the values measured before and after annealing, respectively. The error on the measurement is in the order of ± $5{\cdot}10^4$ cm^{-1}.

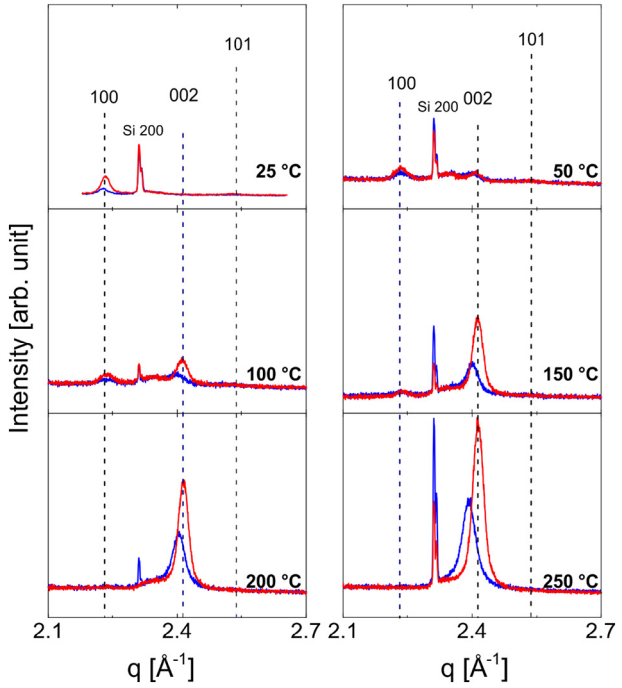

Fig. 7. XRD measurements of the ZnO layers before (blue line) and after (red line) annealing at 600 °C for PE-ALD ZnO layers deposited at different temperatures. The deposition temperatures are reported on the plot. The main crystallographic orientations of ZnO are also reported. The dotted lines show the position and relative intensity of a reference ZnO powder sample (26170-ICSD) [39].

From Bragg's law

$$d_{hkl} = \frac{\lambda}{2\sin(\theta_{hkl})}, \tag{5}$$

with λ = 1.5406 Å the wavelength of Cu Kα radiation, the lattice parameters a and c can then be calculated from the Bragg peaks originating from the (100) and (002) planes:

$$a = \frac{\lambda}{\sqrt{3}\sin\theta_{100}}; \; c = \frac{\lambda}{\sin\theta_{002}} \tag{6}$$

In Table 2, the values of the calculated lattice constants are reported as a function of the deposition temperature before and after annealing.

The lattice constants for pure ZnO are reported in the range a = 3.2475–3.2501 and c = 5.2042–5.2075 [6]. The ZnO deposited by PE-ALD has generally a larger lattice constant for both a and c. The presence of grain boundaries, defects and amorphous regions accounts for the uniform lattice expansion. After annealing, the removal of (part) of the defects in the ZnO structure leads to a uniform shrinking of the lattice plane distances, closer to the pure ZnO wurtzite structure. Residual stress in thin films can also be calculated from the position of the XRD Bragg peaks [46]. For ZnO thin films, the stress was derived from:

$$\sigma = -233\left(\frac{c_{bulk} - c_{film}}{c_{bulk}}\right), \tag{7}$$

where c_{bulk} is the strain free lattice constant and c_{film} is the lattice constant calculated from the XRD Bragg peak. The residual stress before and after annealing is reported in Table 2. Compressive stress is generally present in the ZnO layers after deposition [47]. The annealing procedure reduces the overall compressive stress, in some cases introducing tensile stress in the layers. It is worth noticing that the 100 crystallites show a lower interplanar spacing compared to the pure ZnO and a residual tensile stress. The (100) preferential growth with its planes parallel to the substrate has been reported with a higher surface free energy than the (002) planes [41]. At high temperatures, the 100 intensity becomes very small, eventually disappearing between 150 °C and 200 °C. The small dimension and the high energy could account for the different residual stress when compared to the 002 crystallites.

In summary, the *in situ* and *ex situ* characterization of the ZnO layers deposited at high temperature upon annealing revealed additional differences among the layers as a function of the deposition temperature. Defects and contamination are present in all ZnO layers, but as a function of the deposition temperature, different sources of defects are present, loosely bound at low deposition temperatures. Upon annealing, the optical quality of the layers was found to increase, with minor effects for the ZnO deposited at higher temperatures. On the contrary, increase in the overall crystallinity was found for layers deposited at higher temperature and with a strong 002 preferential orientation.

Table 2
Values of the ZnO wurtzite lattice constants a and c before and after annealing and the residual stress σ for the PE-ALD ZnO deposited at different temperatures.

Deposition T [°C]	a [Å] (± 0.005)		c [Å] (± 0.005)		σ_{100} [MPa] (± 0.02)		σ_{002} [MPa] (± 0.02)	
	Before	After	Before	After	Before	After	Before	After
25	3.255	3.248			−0.41	0.16		
50	3.242	3.245	5.244	5.229	0.56	0.35	−1.65	−1.02
100	3.255	3.242	5.249	5.214	0.46	0.56	−1.88	−0.31
150	3.244	3.239	5.239	5.208	0.44	0.78	−1.46	−0.08
200			5.231	5.205			−1.08	0.05
250			5.256	5.206			−2.18	0.03

4. Conclusions

The effect of annealing in air on the optical, chemical and structural properties of ZnO thin films deposited by plasma enhanced atomic layer deposition was investigated in detail, with the aim of enhancing the opto-chemical and structural material properties. The layers were annealed up to 600 °C. *In situ* spectroscopic ellipsometry and X-ray diffraction were adopted to investigate the material properties of room temperature deposited ZnO during the annealing procedure. The combination of the two *in situ* methods identified temperature windows for the removal of adsorbed species and contaminants (such as carbon contaminations, water and Zn-hydroxyl groups, Zone I and II) and for the recrystallization/densification of the materials (Zone III). Between 200 °C and 300 °C removal of contaminants occurs. SE showed thickness loss and increase in the refractive index, together with an increase in the absorption coefficient (at 375 nm) of the ZnO layers. No change in the structure of the layer was witnessed with XRD, which pointed out the sole removal of impurities from the ZnO layers. Starting at 360 °C till 500 °C, major structural and optical changes were measured, identifying this temperature window as critical for ZnO-based applications. Densification of the layer and increase in crystallinity were observed, leading in turn to a higher material quality. Near-bandgap absorption was found to drastically decrease leading to sharper optical bandgap. The *in situ* investigation was corroborated by *ex situ* characterization of the ZnO layers, at different stages of the annealing procedure, showing the tunability of the ZnO optical and structural properties as a function of the annealing temperature.

The study was extended to PE-ALD ZnO layers deposited at higher temperatures. The combination of *in situ* and *ex situ* analyses highlighted the presence of differences among the ZnO layers in terms of contaminations/defects and structural properties, prior the annealing. Removal of loosely bound contamination was observed for layers deposited up to 100 °C. With higher deposition temperatures, minor effects of the annealing procedure up to 360 °C were found. At this temperature, recrystallization and densification of the materials

occurred, independent of the deposition conditions. Residual stress calculations measured from the XRD diffractograms showed the reduction of the total compressive stress upon annealing. The absorption coefficient (at 375 nm) was found to increase after annealing, with an effect proportional to the initial optical quality of the ZnO. An increased O/Zn ratio was measured with XPS, pointing out only increased amount of oxygen provided during annealing.

Overall, the investigation highlights different aspects of the PE-ALD ZnO thin films, which have been increasingly adopted for cutting-edge opto-electrical devices. The *in situ* characterization highlighted important differences among layers processed with increasing deposition temperatures and the impact of specific annealing temperature windows on the material characteristics, suggesting the post-deposition annealing as a valuable tool to add specific properties to the material that are not achievable by depositing at higher temperature.

Notes

The authors declare no competing financial interest.

Acknowledgments

The authors would like to thank S. Pachmajer (Graz University of Technology, Graz, Austria) for the *in situ* XRD measurements and the fruitful data discussion. This project has received funding from the European Research Council (ERC) under the European Union's Horizon 2020 research and innovation program (grant agreement 715403).

Appendix A. Supplementary data

Supplementary data to this article can be found online at https://doi.org/10.1016/j.apsusc.2019.03.122.

References

[1] X. Yu, T.J. Marks, A. Facchetti, Metal oxides for optoelectronic applications, Nat. Mater. 15 (4) (2016) 383–396, https://doi.org/10.1038/nmat4599.
[2] C. Klingshirn, J. Fallert, H. Zhou, J. Sartor, C. Thiele, F. Maier-Flaig, D. Schneider, H. Kalt, 65 years of ZnO research - old and very recent results, Phys. Status Solidi 247 (6) (2010) 1424–1447, https://doi.org/10.1002/pssb.200983195.
[3] T. Tynell, M. Karppinen, Atomic layer deposition of ZnO: a review, Semicond. Sci. Technol. 29 (4) (2014) 043001, , https://doi.org/10.1088/0268-1242/29/4/043001.
[4] S.K. Arya, S. Saha, J.E. Ramirez-Vick, V. Gupta, S. Bhansali, S.P. Singh, Recent advances in ZnO nanostructures and thin films for biosensor applications: review, Anal. Chim. Acta 737 (2012) 1–21, https://doi.org/10.1016/j.aca.2012.05.048.
[5] C. Cachoncinlle, C. Hebert, J. Perrière, M. Nistor, A. Petit, E. Millon, Random lasing of ZnO thin films grown by pulsed-laser deposition, Appl. Surf. Sci. 336 (2015) 103–107, https://doi.org/10.1016/J.APSUSC.2014.09.186.
[6] Ü. Özgür, Y.I. Alivov, C. Liu, A. Teke, M.A. Reshchikov, S. Doğan, V. Avrutin, S.-J. Cho, H. Morkoç, A comprehensive review of ZnO materials and devices, J. Appl. Phys. 98 (4) (2005) 041301, , https://doi.org/10.1063/1.1992666.
[7] Y. Wu, P.M. Hermkens, B.W.H. van de Loo, H.C.M. Knoops, S.E. Potts, M.A. Verheijen, F. Roozeboom, W.M.M. Kessels, Electrical transport and Al doping efficiency in nanoscale ZnO films prepared by atomic layer deposition, J. Appl. Phys. 114 (2) (2013) 024308, , https://doi.org/10.1063/1.4813136.
[8] D.-J. Lee, H.-M. Kim, J.-Y. Kwon, H. Choi, S.-H. Kim, K.-B. Kim, Structural and electrical properties of atomic layer deposited Al-doped ZnO films, Adv. Funct. Mater. 21 (3) (2011) 448–455, https://doi.org/10.1002/adfm.201001342.
[9] L. Zhu, W. Zeng, Room-temperature gas sensing of ZnO-based gas sensor: a review, Sensors Actuators A Phys. 267 (2017) 242–261, https://doi.org/10.1016/j.sna.2017.10.021.
[10] D. Kim, H. Kang, J.M. Kim, H. Kim, The properties of plasma-enhanced atomic layer deposition (ALD) ZnO thin films and comparison with thermal ALD, Appl. Surf. Sci. 257 (8) (2011) 3776–3779, https://doi.org/10.1016/j.apsusc.2010.11.138.
[11] M. Baitimirova, R. Viter, J. Andzane, A. van der Lee, D. Voiry, I. Iatsunskyi, E. Coy, L. Mikoliunaite, S. Tumenas, K. Załęski, et al., Tuning of structural and optical properties of graphene/ZnO Nanolaminates, J. Phys. Chem. C 120 (41) (2016) 23716–23725, https://doi.org/10.1021/acs.jpcc.6b07221.
[12] O. Graniel, M. Weber, S. Balme, P. Miele, M. Bechelany, Atomic layer deposition for biosensing applications, Biosens. Bioelectron. 122 (2018) 147–159, https://doi.org/10.1016/j.bios.2018.09.038.
[13] A. Abou Chaaya, R. Viter, M. Bechelany, Z. Alute, D. Erts, A. Zalesskaya, K. Kovalevskis, V. Rouessac, V. Smyntyna, P. Miele, Evolution of microstructure and related optical properties of ZnO grown by atomic layer deposition, Beilstein J. Nanotechnol. 4 (1) (2013) 690–698, https://doi.org/10.3762/bjnano.4.78.
[14] F.B. Oruc, L.E. Aygun, I. Donmez, N. Biyikli, A.K. Okyay, H.Y. Yu, Low temperature atomic layer deposited ZnO photo thin film transistors, J. Vac. Sci. Technol. A Vacuum, Surfaces, Film. 33 (1) (2015) 01A105, https://doi.org/10.1116/1.4892939.
[15] A. Tereshchenko, M. Bechelany, R. Viter, V. Khranovskyy, V. Smyntyna, N. Starodub, R. Yakimova, Optical biosensors based on ZnO nanostructures: advantages and perspectives. A review, Sensors Actuators B Chem. 229 (2016) 664–677, https://doi.org/10.1016/j.snb.2016.01.099.
[16] P.C. Rowlette, C.G. Allen, O.B. Bromley, A.E. Dubetz, C.A. Wolden, Plasma-enhanced atomic layer deposition of semiconductor grade ZnO using dimethyl zinc, Chem. Vap. Depos. 15 (1–3) (2009) 15–20, https://doi.org/10.1002/cvde.200806725.
[17] J. Pilz, A. Perrotta, P. Christian, M. Tazreiter, R. Resel, G. Leising, T. Griesser, A.M. Coclite, Tuning of material properties of ZnO thin films grown by plasma-enhanced atomic layer deposition at room temperature, J. Vac. Sci. Technol. A Vacuum, Surfaces, Film. 36 (1) (2018) 01A109, , https://doi.org/10.1116/1.5003334.
[18] J.-L. Tian, H.-Y. Zhang, G.-G. Wang, X.-Z. Wang, R. Sun, L. Jin, J.-C. Han, Influence of film thickness and annealing temperature on the structural and optical properties of ZnO thin films on Si (100) substrates grown by atomic layer deposition, Superlattice. Microst. 83 (2015) 719–729, https://doi.org/10.1016/j.spmi.2015.03.062.
[19] H. Zheng, R.-J. Zhang, J.-P. Xu, S.-X. Wang, T.-N. Zhang, Y. Sun, Y.-X. Zheng, S.-Y. Wang, X. Chen, L.-Y. Chen, et al., Thickness-dependent optical constants and annealed Phase transitions of ultrathin ZnO films, J. Phys. Chem. C 120 (39) (2016) 22532–22538, https://doi.org/10.1021/acs.jpcc.6b06173.
[20] H. Liu, R. Bin Yang, S. Guo, C.J.J. Lee, N.L. Yakovlev, Effect of annealing on structural and optical properties of ZnO/Al2O3superlattice structures grown by atomic layer deposition at 150 °C, J. Alloys Compd. 703 (2017) 225–231, https://doi.org/10.1016/j.jallcom.2017.01.305.
[21] C.Y. Yen, S.R. Jian, G.J. Chen, C.M. Lin, H.Y. Lee, W.C. Ke, Y.Y. Liao, P.F. Yang, C.T. Wang, Y.S. Lai, et al., Influence of annealing temperature on the structural, optical and mechanical properties of ALD-derived ZnO thin films, Appl. Surf. Sci. 257 (17) (2011) 7900–7905, https://doi.org/10.1016/j.apsusc.2011.04.088.
[22] N. Biyikli, A. Haider, Atomic layer deposition: an enabling Technology for the Growth of functional nanoscale semiconductors, Semicond. Sci. Technol. 32 (9) (2017) 093002, , https://doi.org/10.1088/1361-6641/aa7ade.
[23] C. Marichy, M. Bechelany, N. Pinna, Atomic layer deposition of nanostructured materials for energy and environmental applications, Adv. Mater. 24 (8) (2012) 1017–1032, https://doi.org/10.1002/adma.201104129.
[24] C. Marichy, N. Pinna, Atomic layer deposition to materials for gas sensing applications, Adv. Mater. Interfaces 3 (21) (2016), https://doi.org/10.1002/admi.201600335.
[25] J.T. Korhonen, P. Hiekkataipale, J. Malm, M. Karppinen, O. Ikkala, R.H.A. Ras, Inorganic hollow nanotube aerogels by atomic layer deposition onto native Nanocellulose templates, ACS Nano 5 (3) (2011) 1967–1974, https://doi.org/10.1021/nn200108s.
[26] H.C.M. Knoops, B.W.H. van de Loo, S. Smit, M.V. Ponomarev, J.-W. Weber, K. Sharma, W.M.M. Kessels, M. Creatore, Optical modeling of plasma-deposited ZnO films: Electron scattering at different length scales, J. Vac. Sci. Technol. A Vacuum, Surfaces, Film. 33 (2) (2015) 021509, , https://doi.org/10.1116/1.4905086.
[27] B.D. Viezbicke, S. Patel, B.E. Davis, D.P. Birnie, Evaluation of the Tauc method for optical absorption edge determination: ZnO thin films as a model system, Phys. Status Solidi 252 (8) (2015) 1700–1710, https://doi.org/10.1002/pssb.201552007.
[28] P. Christian, A.M. Coclite, Vapor-Phase-synthesized Fluoroacrylate polymer thin films: thermal stability and structural properties, Beilstein J. Nanotechnol. 8 (1) (2017) 933–942, https://doi.org/10.3762/bjnano.8.95.
[29] C.D. Wanger, W.M. Riggs, L.E. Davis, J.F. Moulder, G.E. Muilenberg, Handbook of X-Ray Photoelectron Spectroscopy, Eden Prairie, Minnesota, USA (1979), https://doi.org/10.1002/sia.740030412.
[30] J. Laube, D. Nübling, H. Beh, S. Gutsch, D. Hiller, M. Zacharias, Resistivity of atomic layer deposition grown ZnO: the influence of deposition temperature and post-annealing, Thin Solid Films 603 (2016) 377–381, https://doi.org/10.1016/J.TSF.2016.02.060.
[31] I.-W. Kim, K.-M. Lee, Evaporation of epitaxial ZnO films during post-deposition annealing, Jpn. J. Appl. Phys. 46 (6A) (2007) 3556–3559, https://doi.org/10.1143/JJAP.46.3556.
[32] I.W. Kim, S.J. Doh, C.C. Kim, J.H. Je, J. Tashiro, M. Yoshimoto, Effect of evaporation on surface morphology of epitaxial ZnO films during postdeposition annealing, Appl. Surf. Sci. 241 (1–2) (2005) 179–182, https://doi.org/10.1016/J.APSUSC.2004.09.087.
[33] T. Jun, K. Song, Y. Jeong, K. Woo, D. Kim, C. Bae, J. Moon, High-performance low-temperature solution-Processable ZnO thin film transistors by microwave-assisted annealing, J. Mater. Chem. 21 (4) (2011) 1102–1108, https://doi.org/10.1039/C0JM02178D.
[34] R.C. Rai, M. Guminiak, S. Wilser, B. Cai, M.L. Nakarmi, Elevated temperature dependence of energy band gap of ZnO thin films grown by E-beam deposition, J. Appl. Phys. 111 (7) (2012) 073511, , https://doi.org/10.1063/1.3699365.
[35] R.C. Rai, Analysis of the Urbach tails in absorption spectra of Undoped ZnO thin films, J. Appl. Phys. 113 (15) (2013) 153508, , https://doi.org/10.1063/1.4801900.
[36] T. Skettrup, Urbach's rule derived from thermal fluctuations in the band-gap energy, Phys. Rev. B 18 (6) (1978) 2622–2631, https://doi.org/10.1103/PhysRevB.18.2622.

[37] L. Wang, N.C. Giles, Temperature dependence of the free-exciton transition energy in zinc oxide by photoluminescence excitation spectroscopy, J. Appl. Phys. 94 (2) (2003) 973–978, https://doi.org/10.1063/1.1586977.
[38] V.R. Rai, V. Vandalon, S. Agarwal, Influence of surface temperature on the mechanism of atomic layer deposition of aluminum oxide using an oxygen plasma and ozone, Langmuir 28 (1) (2012) 350–357, https://doi.org/10.1021/la201136k.
[39] S.C. Abrahams, J.L. Bernstein, Remeasurement of the structure of hexagonal ZnO, Acta Crystallogr. Sect. B: Struct. Crystallogr. Cryst. Chem. 25 (7) (1969) 1233–1236, https://doi.org/10.1107/S0567740869003876.
[40] Z.B. Fang, Z.J. Yan, Y.S. Tan, X.Q. Liu, Y.Y. Wang, Influence of post-annealing treatment on the structure properties of ZnO films, Appl. Surf. Sci. 241 (3–4) (2005) 303–308, https://doi.org/10.1016/J.APSUSC.2004.07.056.
[41] J. Kennedy, P.P. Murmu, J. Leveneur, A. Markwitz, J. Futter, Controlling preferred orientation and electrical conductivity of zinc oxide thin films by post growth annealing treatment, Appl. Surf. Sci. 367 (2016) 52–58, https://doi.org/10.1016/j.apsusc.2016.01.160.
[42] A. Ghosh, N.G. Deshpande, Y.G. Gudage, R.A. Joshi, A.A. Sagade, D.M. Phase, R. Sharma, Effect of annealing on structural and optical properties of zinc oxide thin film deposited by successive ionic layer adsorption and reaction technique, J. Alloys Compd. 469 (1–2) (2009) 56–60, https://doi.org/10.1016/J.JALLCOM.2008.02.061.
[43] O. Lupan, T. Pauporté, L. Chow, B. Viana, F. Pellé, L.K. Ono, B. Roldan Cuenya, H. Heinrich, Effects of annealing on properties of ZnO thin films prepared by electrochemical deposition in chloride medium, Appl. Surf. Sci. 256 (6) (2010) 1895–1907, https://doi.org/10.1016/J.APSUSC.2009.10.032.
[44] D. Verma, A.K. Kole, P. Kumbhakar, Red shift of the band-edge photoluminescence emission and effects of annealing and capping agent on structural and optical properties of ZnO nanoparticles, J. Alloys Compd. 625 (2015) 122–130, https://doi.org/10.1016/J.JALLCOM.2014.11.102.
[45] J. Zhang, H. Yang, Q. Zhang, S. Dong, J.K. Luo, Structural, optical, electrical and resistive switching properties of ZnO thin films deposited by thermal and plasma-enhanced atomic layer deposition, Appl. Surf. Sci. 282 (October) (2013) 390–395, https://doi.org/10.1016/j.apsusc.2013.05.141.
[46] R. Hong, J. Huang, H. He, Z. Fan, J. Shao, Influence of different post-treatments on the structure and optical properties of zinc oxide thin films, Appl. Surf. Sci. 242 (3–4) (2005) 346–352, https://doi.org/10.1016/J.APSUSC.2004.08.037.
[47] T. Singh, T. Lehnen, T. Leuning, D. Sahu, S. Mathur, Thickness dependence of optoelectronic properties in ALD grown ZnO thin films, Appl. Surf. Sci. 289 (2014) 27–32, https://doi.org/10.1016/J.APSUSC.2013.10.071.